RESEARCH DEPARTMENT

Re-radiation from masts and similar obstacles at radio frequencies

RESEARCH REPORT No. E - 118

UDC 621.396.67: 621.391.812.7

1966/24

THE BRITISH BROADCASTING CORPORATION
ENGINEERING DIVISION

RESEARCH DEPARTMENT

RE-RADIATION FROM MASTS AND SIMILAR OBSTACLES AT RADIO FREQUENCIES

Research Report No. E-118
UDC 621.396.67: 1966/24
621.391.812.7

P. Knight, B.A., A.M.I.E.E.

D. Maurice

for Head of Research Department

We therefore consider the arrangement shown in plan in Fig. 2, the distance to A_2 being very much greater than d_1. The resultant field strength at A_2 may be calculated by integrating over the wavefront, to infinity on both sides of the strip; this gives the sum of the direct and re-radiated fields. Alternatively the re-radiated field alone may be calculated by integrating the incident field strength over the width of the strip itself; this procedure may be justified by Babinet's principle. Adopting the latter procedure we obtain the result

$$\rho_0(\pi) = -\sqrt{2}\ \psi(u)\ e^{j\pi/4} \qquad (7)$$

where $u = w/(2\lambda d_1)^{1/2}$, w is the width of the strip and $\psi(u)$ is the complex Fresnel integral,* defined by

$$\psi(u) = C(u) - jS(u) = \int_0^u e^{-j\pi t^2/2}\, dt \qquad (8)$$

It will be noted that $\rho_0(\pi)$ is approximately equal to -1 for very wide obstacles as the re-radiated field tends to cancel the direct radiation but for narrower obstacles (corresponding to small values of u) the phase of the re-radiated field tends towards $-3\pi/4$. In directions other than $\phi = \pi$ the relative phase of the direct and re-radiated signals depends on the separation in wavelengths between the transmitting aerial and the obstacle; the greater the spacing the more rapidly does the phase vary as the observer moves round the system. In most practical arrangements the phase varies so rapidly, both with direction and with frequency, that it is difficult to predict it accurately except in the immediate vicinity of the shadow region. Attention is therefore mainly confined to the relative amplitude of the re-radiated signal, since this sets the upper and lower limits to the resultant field strength. In the shadow region, however, an accurate knowledge of the phase is often desirable because the relative phase partly determines the width of the shadow.

The coefficient $g(\pi)$ for a strip or wide obstacle may be obtained by writing $\phi = \pi$ in Equation (6) and comparing with Equation (7); the result is

$$g(\pi) = (2d_1/\lambda)^{1/2}\ \psi(u) \qquad (9)$$

If $d_1/\lambda > 2(w/\lambda)^2$, $\psi(u)$ is approximately equal** to u and $g(\pi)$ is then equal to w/λ; this result is frequently encountered in situations involving shadowing by obstacles. In directions close to $\phi = \pi$ the re-radiation pattern of the obstacle then resembles that of a uniformly illuminated aperture of width w. A wide obstacle therefore casts a deep shadow over a relatively narrow arc, provided its distance from the transmitting aerial satisfies the criterion $d_1/\lambda > 2(w/\lambda)^2$.

Re-radiation coefficients may be calculated exactly for a few special types of obstacles such as circular cylinders. In other cases approximate theoretical methods may be used with reasonable accuracy. Re-radiation coefficients for obstacles such as lattice masts which are not very amenable to theoretical calculation may be measured with models. A number of different types of obstacles will now be considered in detail.

2.1. Perfectly-Conducting Circular Cylinders

Re-radiation coefficients for perfectly-conducting circular cylinders, for both vertically and horizontally polarized transmissions, are derived in the Appendix (Section 9.1). When $d_2 \gg d_1$ the re-radiation coefficient for vertical polarization* is given by

$$\rho_0(\phi) = -e^{-j\beta d_1 \cos\phi}\left[J_0(\beta a)\,\frac{H_0^{(2)}(\beta d_1)}{H_0^{(2)}(\beta a)} + 2\sum_{n=1}^{\infty} j^n J_n(\beta a)\,\frac{H_n^{(2)}(\beta d_1)}{H_n^{(2)}(\beta a)}\cos n\phi\right] \qquad (10)$$

where a is the radius of the cylinder, J_n denotes the Bessel function of the first kind of order n and $H_n^{(2)}$ denotes the Hankel function of the second kind of order n.

The corresponding expression for horizontal polarization* is

$$\rho_0(\phi) = e^{-j\beta d_1 \cos\phi}\left[J_0'(\beta a)\,\frac{H_0^{(2)}(\beta d_1)}{H_0^{(2)\prime}(\beta a)} + 2\sum_{n=1}^{\infty} j^n J_n'(\beta a)\,\frac{H_n^{(2)}(\beta d_1)}{H_n^{(2)\prime}(\beta a)}\cos n\phi\right] \qquad (11)$$

* It should be noted that Fresnel integrals are sometimes tabulated as a function of u but more often as a function of $\pi u^2/2$, since their values then oscillate with a constant period. In Jahnke and Emde's "Tables of Functions" $\pi u^2/2$ is denoted by z and in Pearcey's "Tables of the Fresnel Integral" by x.

** The error in $\psi(u)$ is 1% in amplitude and 7½° in phase.

* It is convenient to use these terms throughout the report to describe the field incident on the cylinder; we assume that the axis of the cylindrical obstacle is vertical - the usual practical case.

where $J_n'(\beta a)$ and $H_n^{(2)'}(\beta a)$ denote the first derivatives of $J_n(\beta a)$ and $H_n^{(2)}(\beta a)$ respectively. In both cases the coefficients of cos $n\phi$ diminish as n increases, the number of significant terms in the series depending on the cylinder radius.

Equations (10) and (11) are not in a convenient form for the graphical representation of $\rho_0(\phi)$ since this is a function of three variables (a, d_1 and ϕ); nevertheless a limited range of curves has been published.[8] However, if $d_1/\lambda > 2{\cdot}2(2a/\lambda)^2$, the Hankel functions of βd_1 may be replaced by their asymptotic values in all the significant terms* of the expansions and the expressions for $\rho_0(\phi)$ then take the same form as Equation (6) and lead to the following value for $g(\phi)$ when the electric vector is parallel to the cylinder axis (vertical polarization).

$$g(\phi) = \frac{1}{\pi}\left[\frac{J_0(\beta a)}{H_0^{(2)}(\beta a)} + 2\sum_{n=1}^{\infty}(-1)^n \frac{J_n(\beta a)}{H_n^{(2)}(\beta a)} \cos n\phi\right] \quad (12)$$

The corresponding result for horizontal polarization is

$$g(\phi) = -\frac{1}{\pi}\left[\frac{J_0'(\beta a)}{H_0^{(2)'}(\beta a)} + 2\sum_{n=1}^{\infty}(-1)^n \frac{J_n'(\beta a)}{H_n^{(2)'}(\beta a)} \cos n\phi\right] \quad (13)$$

The modulus of $g(\phi)$ is shown in Fig. 3 as a function of cylinder radius, for three values of ϕ and both polarizations. In Figs. 4 and 5 computed** values of $|g(\phi)|$ are plotted as a function of ϕ for three cylinder radii; these curves are therefore horizontal re-radiation patterns. It will be seen that the re-radiated field is substantially constant between $\phi = 0$ and 120° because, for these directions, the obstacle is behaving as a cylindrical mirror. In the direction $\phi = 180°$ the re-radiated field rises to a much larger value and the h.r.p. has a lobe whose width decreases as the cylinder size increases. In this direction the contributions to the re-radiated field from all the induced currents on the cylinder tend to be in phase and, as with any co-phased aperture distribution, the width of the main lobe decreases as the aperture increases.

It is of interest to compare these values of $|g(\phi)|$ with those which would be obtained by the methods of geometrical optics. Over a wide arc centred on the direction $\phi = 0$ the cylinder may be regarded as a cylindrical mirror and in the Appendix (Section 9.2) it is shown that $|g(\phi)|$ is then given approximately by

$$|g(\phi)| \simeq \frac{1}{2}\left[\frac{2a}{\lambda}\cos\frac{\phi}{2}\right]^{1/2} \quad (14)$$

Values calculated from this expression for $\phi = 0$ and 90° are shown in Fig. 3 and the agreement with the exact values is surprisingly good in view of the small cylinder radii considered. With larger cylinders the agreement is even better; for $\beta a = 20$ the approximate values for $|g(\phi)|$ are almost indistinguishable from the exact values shown in Fig. 4 for values of ϕ up to 120°.

In the direction $\phi = 180°$ (the shadow region) the cylinder may be regarded as equivalent to a flat strip of width $2a$, for which $|g(\phi)| \simeq 2a/\lambda$. This value of $|g(\phi)|$ is also shown in Fig. 3 and, again, agreement is obtained. In Fig. 5 the re-radiation pattern of a strip* is compared with the exact re-radiation patterns of a cylinder of 20 radians radius for both polarizations; it will be seen that the shapes of the lobes centred on $\phi = 180°$ are accurately reproduced by the strip approximation.

These results show that the methods of geometrical optics may be used with little error for cylinders more than 2λ in diameter. They also show that, for cylinders exceeding this size, $\rho_0(\phi)$ is independent of frequency over a wide arc centred on $\phi = 0$, but proportional to the square root of the frequency in the shadow direction.

* The term whose amplitude is 10% of the largest term preceeding it has a phase error of 22½°; subsequent terms have greater phase errors but smaller amplitudes. It will be noted that the criterion stated above is almost the same as that given below Equation (9).

** The computer programmes for these functions, and for other functions discussed later in this report, were written by R.W. Lee and R.E. Davies.

* The current induced on the strip is assumed to be co-phased across the width, w, of the strip; this corresponds to the condition $(d_1/\lambda) \gg (w/\lambda)^2$. The strip patterns are therefore strictly comparable with the cylinder patterns since the latter are exact when d_1 is very large. The effect of decreasing d_1 is to slightly fill the zeros of the strip pattern.

When $d_2 \gg d_1$ the relative phase of the re-radiated and direct signals is given by Equation (6). When the spacing between the transmitting aerial and cylinder is large enough for Equations (12) and (13) to apply, the phase of $\rho_0(\phi)$ in the direction $\phi = 180°$ is

$$\Phi\{\rho_0(\pi)\} = \Phi\left\{\frac{J_0(\beta a)}{H_0^{(2)}(\beta a)} + 2\sum_{n=1}^{\infty}\frac{J_n(\beta a)}{H_n^{(2)}(\beta a)}\right\} - \frac{3\pi}{4} \quad (15)$$

for vertical polarization

$$\Phi\{\rho_0(\pi)\} = \Phi\left\{\frac{J_0'(\beta a)}{H_0^{(2)'}(\beta a)} + 2\sum_{n=1}^{\infty}\frac{J_n'(\beta a)}{H_n^{(2)'}(\beta a)}\right\} + \frac{\pi}{4} \quad (16)$$

for horizontal polarization

where $\Phi(x)$ signifies the phase of x.

Fig. 6 shows how the relative phase in the direction $\phi = 180°$ varies with cylinder radius. For both polarizations the phase tends to -135° as the cylinder radius increases; this value is consistent with that which would be obtained by the methods of geometrical optics.

2.2. Perfectly-Conducting Polygonal Cylinders

This Section deals with square- and triangular-section cylinders and therefore covers the types of mast structures commonly encountered. The surfaces of the cylinders are assumed to be perfectly conducting or to be covered with sufficient screening wires to make the surface impedance small compared with the intrinsic impedance of free space. Open lattice structures are considered separately in Section 2.3.

When the width of an obstacle is small compared with the wavelength it may be replaced by an equivalent circular cylinder and the results of Section 2.1 applied. In calculating the size of the equivalent circular cylinder we assume for vertical polarization that the polygonal cylinder forms the inner conductor of a hypothetical transmission line having a large outer conductor; the radius of the equivalent circular cylinder is then such that, if substituted for the polygon, no change in characteristic impedance occurs. It has been shown [9,10] that square and triangular cylinders with sides of width w may be replaced by circular cylinders of radii $0{\cdot}59w$ and $0{\cdot}42w$ respectively and that a flat strip of width w is equivalent to a circular cylinder of radius $w/4$. There is, however, no justification for the use of this method for horizontal polarization because the re-radiation coefficient depends on the orientation of the cylinder relative to the direction of the incident radiation; this is apparent from consideration of a flat strip. Nevertheless the approximations stated above appear to be reasonably accurate for regular polygons.*

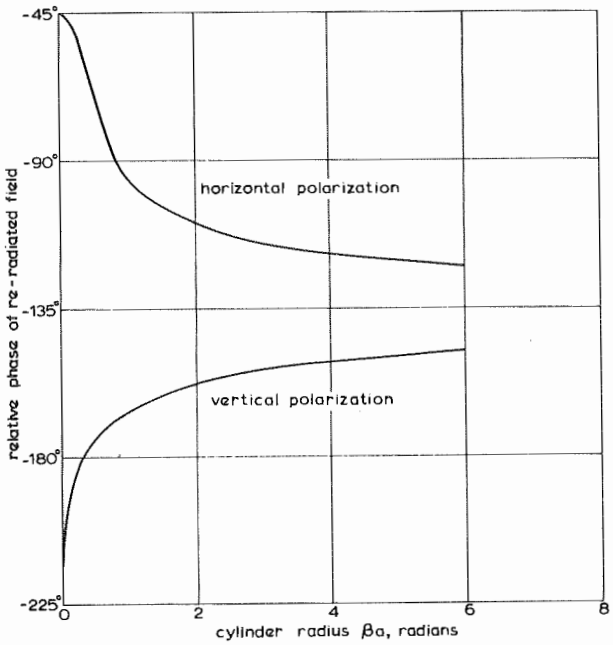

Fig. 6 - Relative phase of re-radiation from a circular cylinder in direction $\phi = \pi$

When the width of a polygonal cylinder is large compared with the wavelength, its illuminated faces tend to behave as plane mirrors and the re-radiation coefficient may be calculated by the methods of geometrical optics. Thus the square-section cylinder shown in Fig. 7 will re-radiate strongly in directions P and R. The intensity of reflected wave will be approximately equal to that of the incident wave if the transmitting aerial is so

* From published curves[3] showing the scattering cross-section of small rectangular cylinders it may be shown that a square cylinder of width w scatters the same power as a circular cylinder of radius $0{\cdot}68w$ when one face is normal to the direction of incidence of a horizontally polarized wave.

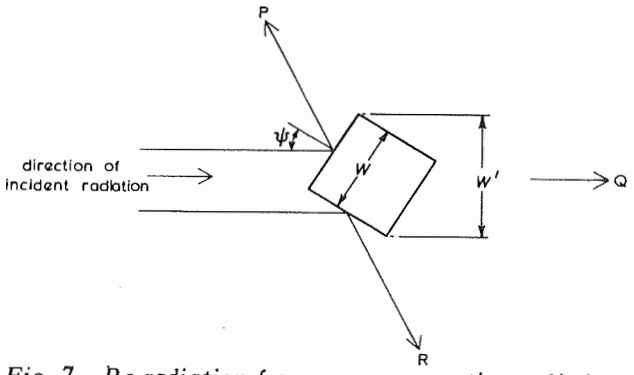

Fig. 7 - Re-radiation from a square-section cylinder

close that the whole of the first Fresnel zone* lies on the reflecting surface. If this condition is not satisfied the intensity of the reflected wave will be reduced. If the width of the obstacle is small compared with the distance to the transmitter the use of the coefficient $g(\phi)$ is valid and its modulus may be shown to be equal to the projected width of the reflecting surface in wavelengths. Thus in the direction P in Fig. 7, $|g(\phi)| = (w/\lambda)\cos\psi$ and the horizontal re-radiation pattern of the cylinder has a lobe which resembles that of a uniform aperture of width $(w/\lambda)\cos\psi$. In the direction Q, $|g(\pi)|$ is equal to the projected width (w') of the cylinder in wavelengths and the horizontal re-radiation pattern has a main lobe which resembles that of a uniform aperture of width w'/λ.

* This condition is satisfied when the path lengths of non-specular rays travelling via the edges of the reflecting surface exceed the path length of the specularly-reflected ray by more than $\lambda/2$.

When the polygon is of intermediate size there appears to be no justification for the use of either the equivalent circular cylinder method or the geometric-optics approximation. A more exact theoretical approach using an integral equation method has been described in a paper[4] which contains computed re-radiation characteristics for square- and rectangular-section cylinders and $|g(\phi)|$ may be derived from these characteristics in the manner described in the Appendix (Section 9.3). In Fig. 8, values of $|g(\phi)|$ derived for waves normally incident on square-section cylinders are compared with values calculated by the two approximate methods. It will be seen that in the direction $\phi = 0$ the equivalent circular cylinder approximation is inaccurate

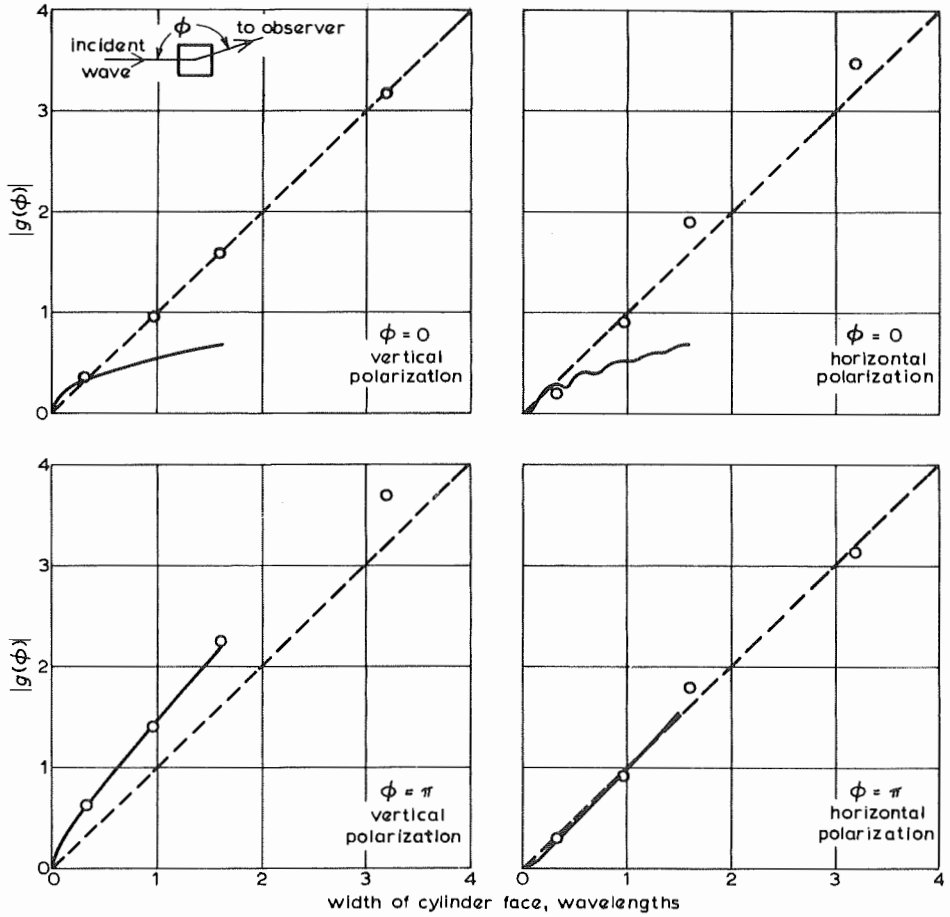

Fig. 8 - Re-radiation coefficient of square-section cylinders of intermediate size

o Value derived from Reference 4

——— Equivalent cylinder approximation, from Fig. 3 — — — Geometric optics approximation

for square-section cylinders more than 0·5λ wide; above this width the geometric-optics method may be used with confidence. In the shadow region ($\phi = 180°$) both of the approximate methods yield similar results and agree reasonably well with the more exact method.

Reference 4 contains a number of computed power re-radiation patterns for square- and rectangular-section cylinders which show clearly the way in which the cylinder faces tend to behave as plane mirrors as the cylinder size increases. They also show how the widths of the re-radiation lobes are reduced as the cylinder size increases.

2.3. Lattice Masts

The methods described in Section 2.2 cannot be used for unscreened lattice masts which are more than a small fraction of a wavelength wide because the spaces between their structural members are an appreciable fraction of a wavelength. The re-radiation coefficient of such a mast depends to some extent on the number and arrangement of its cross bracings and is difficult to calculate theoretically.

Because of this difficulty a comprehensive series of measurements[5] has been carried out on models of typical square-section lattice masts up to 2 wavelengths wide. Re-radiation coefficients were measured for all values of ϕ, for both polarizations. The model masts were oriented first with a face normal to, and then at 45° to, the direction of the incident radiation.

The measured re-radiation coefficients showed considerable variation with mast size, orientation and receiving aerial direction. With vertical polarization the results were consistent with re-radiation from currents induced in the corner pillars of the masts and it was found possible to calculate re-radiation coefficients with reasonable accuracy by regarding the mast as four parallel conducting cylinders. With horizontal polarization, variations due to currents induced in the corner pillars could still be distinguished although they were partly obscured by re-radiation from the cross bracings. The calculation of re-radiation coefficients was not considered to be practicable for horizontal polarization.

With horizontal polarization (and to a lesser extent with vertical polarization) the re-radiation coefficient depends to a considerable extent on the number and disposition of the cross bracings. Consequently the detailed measurements described apply only to the particular type of lattice structure which was investigated although the maximum values of the measured re-radiation coefficients are a reliable guide to the maximum values which are likely to be encountered with any similar type of structure. It was observed that these maxima were approximately equal to the corresponding values for the equivalent circular cylinder described in Section 2.2 and it is therefore proposed that the equivalent circular cylinder should be used as a basis for calculating upper limits to re-radiation coefficients, even though there is no theoretical justification for this procedure.

2.4. Imperfectly-Conducting Cylinders

In this section we consider the effects of obstacles such as tall buildings, factory chimneys and concrete towers. With an imperfectly-conducting obstacle the induced currents are not confined to the surface (as with a perfect conductor) but are distributed in the surface layer. The current density decreases exponentially, having a value which is 37% of that at the surface at a depth called the penetration depth. If the thickness of the obstacle is at least four times the penetration depth the incident wave will be attenuated by 35 dB by the time it reaches the far side of the obstacle. The obstacle is then almost completely opaque and does not differ, insofar as the field beyond it is concerned, from a perfectly-conducting obstacle.

With perfectly-conducting obstacles we may regard the resultant field strength in any direction as the vector sum of incident and re-radiated fields; beyond the obstacle the two fields tend to cancel. This approach is equally valid for imperfectly-conducting obstacles* and we can explain their behaviour on this basis. In this case the induced currents are progressively retarded in phase below the surface but, beyond the obstacle, their contributions to the re-radiated field combine in phase. Provided the obstacle is of sufficient thickness the total induced current is approximately equal to that induced on the surface of a perfect conductor and the resultant field beyond the obstacle is indistinguishable from that which would be obtained with a perfect conductor.

The same reasoning may be used to explain why the plane-wave reflexion coefficient of an imperfect conductor is less than unity. In front of the obstacle the contributions from the currents below the surface are not co-phased and the resultant re-radiated field is less than it would be with a perfect conductor.

Although the foregoing argument applies strictly to an infinite plane sheet of material, it is

* More precisely, obstacles whose conductivity in mhos/metre is appreciably greater than $\epsilon F \times 10^{-4}$, where ϵ is the dielectric constant and F the frequency in Mc/s.

approximately correct for any cylinder which is sufficiently large for the methods of geometrical optics to be used. In these cases, therefore, provided the thickness of the cylinder is more than four times the penetration depth, the re-radiation coefficient in the shadow direction may be taken as equal to the value for a perfect conductor. In other directions the re-radiation coefficient for a perfectly-conducting cylinder should be multiplied by the appropriate plane-wave reflexion coefficient.

The majority of imperfectly-conducting structures are made of brick or concrete and these are believed to have similar electrical properties. Reflexion coefficients and penetration depths at 200 Mc/s for wet and dry concrete, estimated from complex permittivity measurements made at h.f.,[11] are contained in Table 1; these values are almost independent of frequency over the whole of the v.h.f. and u.h.f. spectrum.*

We are normally concerned with the greatest re-radiation effect. This occurs when the concrete is wet and under this condition we may regard any brick or concrete structure more than 10 ft (3 m) thick as equivalent to a metallic obstacle so far as shadowing is concerned. The amplitudes of the reflected signals may be taken as equal to half the amplitudes for similar metallic obstacles.

* In making these estimates the real part of the complex permittivity was assumed to be constant and the imaginary part inversely proportional to frequency. For lossy dielectrics the penetration depth is independent of frequency.

The behaviour of reinforced concrete is somewhat different. In the shadow direction the reinforcing rods cause all sizes of structures to behave as metallic obstacles. The reinforcing rods also increase the amplitudes of the reflected signals but it should be noted that the reflexion coefficient for a plane wave incident on a slab of reinforced concrete is not necessarily unity because some attenuation occurs in the surface layer of concrete. In Table 2, plane wave reflexion coefficients are given* for a sheet of concrete with reinforcing rods buried 4 in. (0·1 m) below the surface.

If we again consider the greatest re-radiation effect we find that the reflexion coefficient of reinforced concrete must be assumed to be unity at all frequencies. The conclusion therefore is that reinforced concrete structures must always be considered as equivalent to metallic obstacles.

3. RE-RADIATION FROM OBSTACLES OF FINITE HEIGHT

The re-radiation coefficient of a real obstacle differs from that of a hypothetical infinitely long obstacle partly because of its finite length and partly because of the existence of ground-reflected waves. The re-radiation coefficient of the infinite obstacle is therefore modified by a factor F called the finite obstacle factor; the re-radiation coefficient of the finite obstacle, $\rho(\phi)$, is then given by the expression:

$$\rho(\phi) = F \rho_0(\phi) \qquad (17)$$

* The values given in Table 2 were calculated from Equation (25) of Reference 11.

TABLE 1

Electrical Properties of Concrete

	WET CONCRETE	ALMOST DRY CONCRETE	DRY CONCRETE
Plane wave reflexion coefficient (Normal incidence)	0·50	0·44	0·27
Penetration depth (metres)	0·8	2·3	28

TABLE 2

Plane wave reflexion coefficients for reinforced concrete

	50 Mc/s	200 Mc/s	800 Mc/s
Wet concrete	0·99	0·73	0·63
Almost dry concrete	1·00	0·94	0·91
Dry concrete	1·00	1·00	0·995

In the special case when $d_1 \ll d_2$, this leads to the following simple relationship between $\rho(\phi)$, F and $g(\phi)$.

$$|\rho(\phi)| = |F||g(\phi)|\left(\frac{\lambda}{d_1}\right)^{1/2} \qquad (18)$$

The calculation of $\rho(\phi)$ and F for situations which arise in practice is discussed in this section.

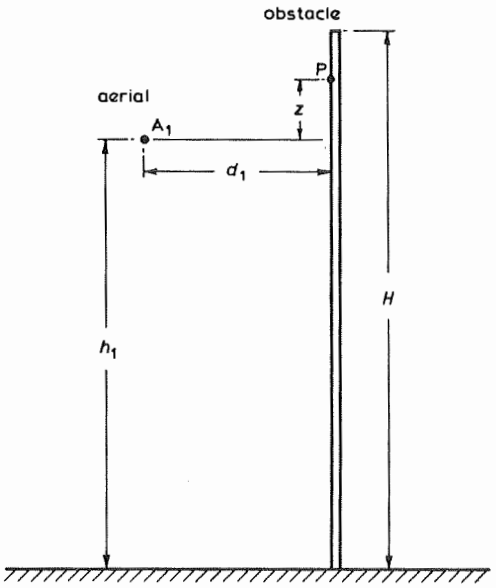

Fig. 9 - An aerial close to a tall obstacle

3.1. Transmitting Aerial Very Close to Obstacle

Fig. 9 shows an aerial A_1 close to a tall obstacle; it represents the situation which can arise if a new mast is erected at an existing transmitting site. In this particular case the ground has no effect, the modification to $\rho_0(\phi)$ depending only on the relative heights of aerial and the top of the obstacle.*

The current induced on the obstacle is greatest at the height of the aerial; above and below this height its amplitude diminishes while its phase becomes progressively retarded. As with the infinite obstacle, the re-radiated field is due mainly to the section of the obstacle for which the phase retardation is less than 180°, i.e. the first Fresnel zone. In general the higher parts of this section will tend to contribute more strongly to the distant field strength than the lower parts on account of height-gain, but if the length of the section corresponding to the first Fresnel zone, $2(\lambda d_1)^{1/2}$, is very much less than h_1 the height-gain variation can be disregarded. Making the usual approximations it follows that the re-radiated field is proportional to

$$\int_{-\infty}^{H-h_1} e^{-j\beta z^2/2d_1}\, dz$$

where z is measured from height h_1 on the obstacle and $d_2 \gg d_1$. It will be noted that the integration has been taken over by the whole of the obstacle even though height-gain and amplitude variations can only be neglected over a limited region. The justification for this depends on the principle of stationary phase, as does the extension of the lower limit of integration to $-\infty$.

The re-radiated field due to an infinite mast in free space is proportional to the same integral taken between infinite limits; the ratio of the two integrals is equal to F, whose modulus is given by

$$|F| = \frac{1}{\sqrt{2}}\,|\psi(u_H - u_h) + \tfrac{1}{2} - j\tfrac{1}{2}| \qquad (19)$$

where

$$u_H = \frac{H/\lambda}{(d/2\lambda)^{1/2}} \qquad u_h = \frac{h/\lambda}{(d/2\lambda)^{1/2}} \qquad (20)$$

$h = h_1$, $d = d_1$ and $\psi(u)$ is the complex Fresnel integral.

The variation of $|F|$ with difference in height between aerial and obstacle is identical with the variation in the intensity of a wave diffracted over a straight edge. Thus $|F| = \frac{1}{2}$ when $H = h_1$. This variation of $|F|$ is shown as a function of $u_H - u_h$ by the $u_A = 0$ curve of Fig. 10. $|F|$ is also a function of the path difference between rays travelling via the top of the obstacle and via the most direct path; this path difference is given in the upper scale of Fig. 10.

If the spacing d_1 is less than 10 wavelengths the validity of Equation (19) becomes questionable. In order to assess the possible error, exact values of $|F|$ for $d_1 = 5\lambda$ were calculated by numerical integration and compared with the curve for $u_A = 0$ in Fig. 10. The error was found to be insignificant provided $|F|$ was expressed as a function of the exact path difference SB - SC (Fig. 10) and not by the approximation $(H-h_1)^2/2d_1$. In other words, reasonably accurate values of $|F|$ may be obtained from Fig. 10 when $d_1 < 10\lambda$ provided the upper horizontal scale is used.

* Although A_1 is assumed to transmit, the results derived in this and subsequent sections are equally valid when A_1 receives, since the principle of reciprocity applies.

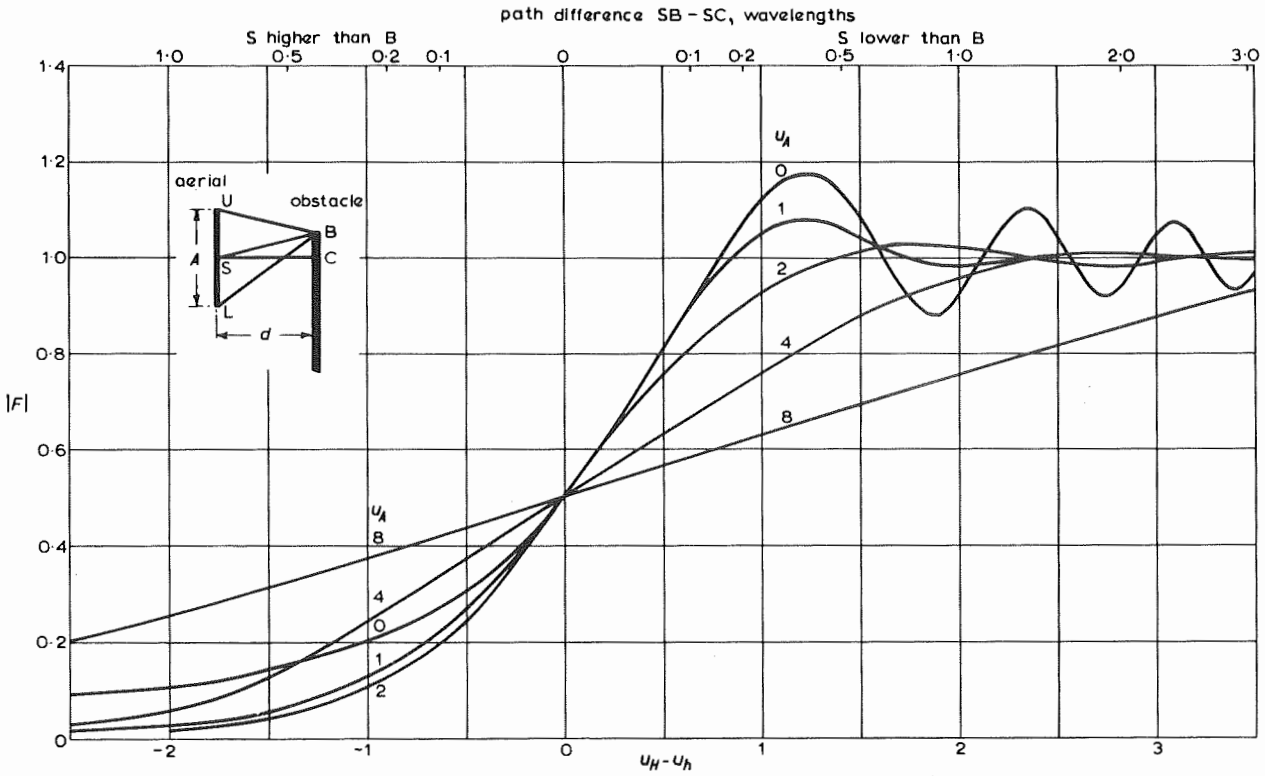

Fig. 10 - Finite obstacle factors for tall obstacles close to aerials having vertical directivity

If the transmitting aerial has a radiating length comparable with $(\lambda d_1)^{1/2}$, F may be smaller for the upper part of the aerial than for the lower; this situation would arise, for example if the centre of the aerial were at the same height as the top of the obstacle. The effective value of $|F|$ for the whole aerial may be obtained by integrating the complex value of F along the length of the aerial and then finding its modulus. Results obtained by numerical integration for a number of cases are shown in Fig. 10; in each case the aerial was assumed to have a constant co-phased current distribution along its radiating length.

3.2. Aerial-to-Obstacle Distance Comparable with Height of Obstacle

If the spacing between the aerial and the obstacle is such that the stationary phase region (i.e. the length $2(\lambda d_1)^{1/2}$, analogous to the first Fresnel zone) extends over an appreciable length of the obstacle, the height-gain variation cannot be disregarded. An additional complication is that the obstacle may be illuminated by ground-reflected radiation in addition to direct radiation, unless the transmitting aerial possesses appreciable vertical directivity.

The height-gain variation is often linear, especially at v.h.f.* In other words, the received field strength, due to re-radiation from a point on the obstacle, is proportional to the height of that point above the ground. Although linear height-gain occurs when d_2 is large, this does not necessarily imply that d_2 is very much greater than d_1. The situation which arises when the height-gain is linear is discussed in Section 3.2.1** and the more general case in Section 3.2.2.

3.2.1. Distant Receiving Aerial, Resulting in Linear Height-Gain over Obstacle

The arrangement considered is shown in Fig. 11(*a*). The obstacle and the two aerials do not necessarily lie in the same vertical plane; thus Fig. 11(*a*) may be regarded as two facing pages of a book which has been fully opened. The distance to the receiving aerial is sufficiently large for the linear height-gain relationship to be satisfied.

* With flat ground the height-gain variation can be regarded as approximately linear up to a height $\lambda d_2/8h_2$, where h_2 is the height of the distant aerial. However, the height-gain variation is frequently influenced by the nature of the path to the distant aerial and consequently the profile of this path should be examined to see if linear height-gain is a reasonable assumption.

** The method described in Section 3.2.1 was originally proposed by G.D. Monteath.

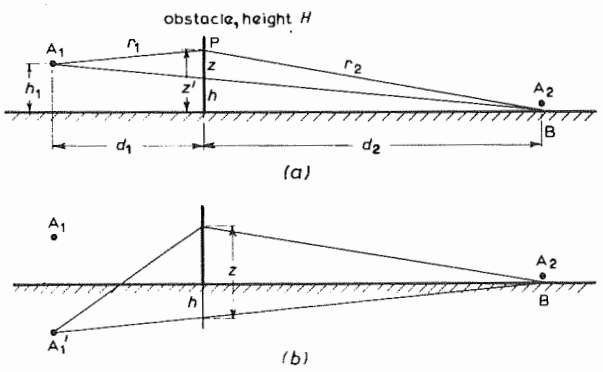

Fig. 11 - An obstacle satisfying the linear height-gain condition

(a) re-radiation due to direct illumination
(b) re-radiation due to ground-reflected illumination

Linear height-gain is taken into account by multiplying Equation (2) by $K'z'$, where K' is a constant and z' is the height of the point P on the obstacle. The re-radiated field strength is therefore

$$E_R = -jK'\,g(\phi)\int_0^H z'\,\frac{e^{-j\beta r_2}}{r_2^{\,2}}\,E(z')\,dz' \qquad (21)$$

where $E(z')$ is the field strength which would exist at the obstacle if the latter were removed. * Since $E(z')$ is the resultant of direct- and ground-reflected radiation from A_1, E_R may be regarded as the sum of two components, each of which may be calculated separately from Equation (1). Thus the component of E_R due to direct radiation is

$$j\,KK'\,g(\phi)\int_{-h}^{H-h}(z+h)\,\frac{e^{-j\beta(r_1+r_2)}}{r_1 r_2^{\,2}}\,dz \qquad (22)$$

where h is the height at which the line A_1B intersects the obstacle, z being measured from the point of intersection, as shown in Fig. 11(*a*). The component E_R due to ground-reflected illumination of the obstacle is calculated by assuming that it originates from a negative image of A_1 in the ground; this implies that the ground reflexion coefficient is -1 at all angles of incidence. This component of E_R is then given by an expression similar to (22) but of opposite sign; for convenience, z is now measured from the intersection of the line $A_1'B$ and the obstacle, as shown in Fig. 11(*b*) and the limits of integration are consequently $H + h$ and h. Addition of these two expressions and the use of approximations for r_1 and r_2 similar to those employed in Section 2 lead to the following result:

$$E_R = -j\,\frac{KK'\,g(\phi)}{d_1 d_2^{\,2}}\,h(\lambda d)^{1/2}\,f(u_H,u_h)\,e^{-j\beta(d_1+d_2+\epsilon)} \qquad (23)$$

where

$$h = h_1 d_2/(d_1+d_2)$$

$$d = d_1 d_2/(d_1+d_2)$$

$$f(u_H,u_h) = \frac{1}{\sqrt{2}}\left[\psi(u_H-u_h)+\psi(u_H+u_h) - \frac{2}{\pi u_h}\,e^{-j\pi(u_H^2+u_h^2)/2}\sin(\pi u_H u_h)\right] \qquad (24)$$

and ϵ is the difference between the length of the straight line A_1B of Fig. 11(*a*) and the horizontal distance $d_1 + d_2$. The quantities u_H and u_h were defined in Equation (20).

The field strength due to direct radiation is

$$E_D = \frac{KK'}{d_0^{\,2}}\,h_1\,e^{-j\beta(d_0+\epsilon_0)} \qquad (25)$$

where ϵ_0 is defined in a similar manner to ϵ. It will be noted that Equation (25) contains a factor $K'h_1$ because the field strength due to direct radiation from A_1 is proportional to h_1. From Equations (23) and (25) we have

$$\rho(\phi) = \frac{E_R}{E_D} = -j\,g(\phi)\,\frac{d_0^{\,2}(\lambda d)^{1/2}}{d_1 d_2(d_1+d_2)} \times f(u_H u_h)\,e^{-j\beta(d_1+d_2-d_0+\epsilon-\epsilon_0)} \qquad (26)$$

Now as $F = \rho(\phi)/\rho_0(\phi)$, from Equations (5) and (26) we have

$$F = \frac{h}{h_1}\,f(u_H,u_h)\,e^{j(\pi/4-\epsilon+\epsilon_0)} \qquad (27)$$

If $d_2 \gg d_1$ Equation (27) simplifies to

$$F = f(u_H,u_h)\,e^{j\pi/4} \qquad (28)$$

* Equation (21) contains the factor $1/r_2^{\,2}$ because field strength is inversely proportional to the square of the distance when linear height-gain applies.

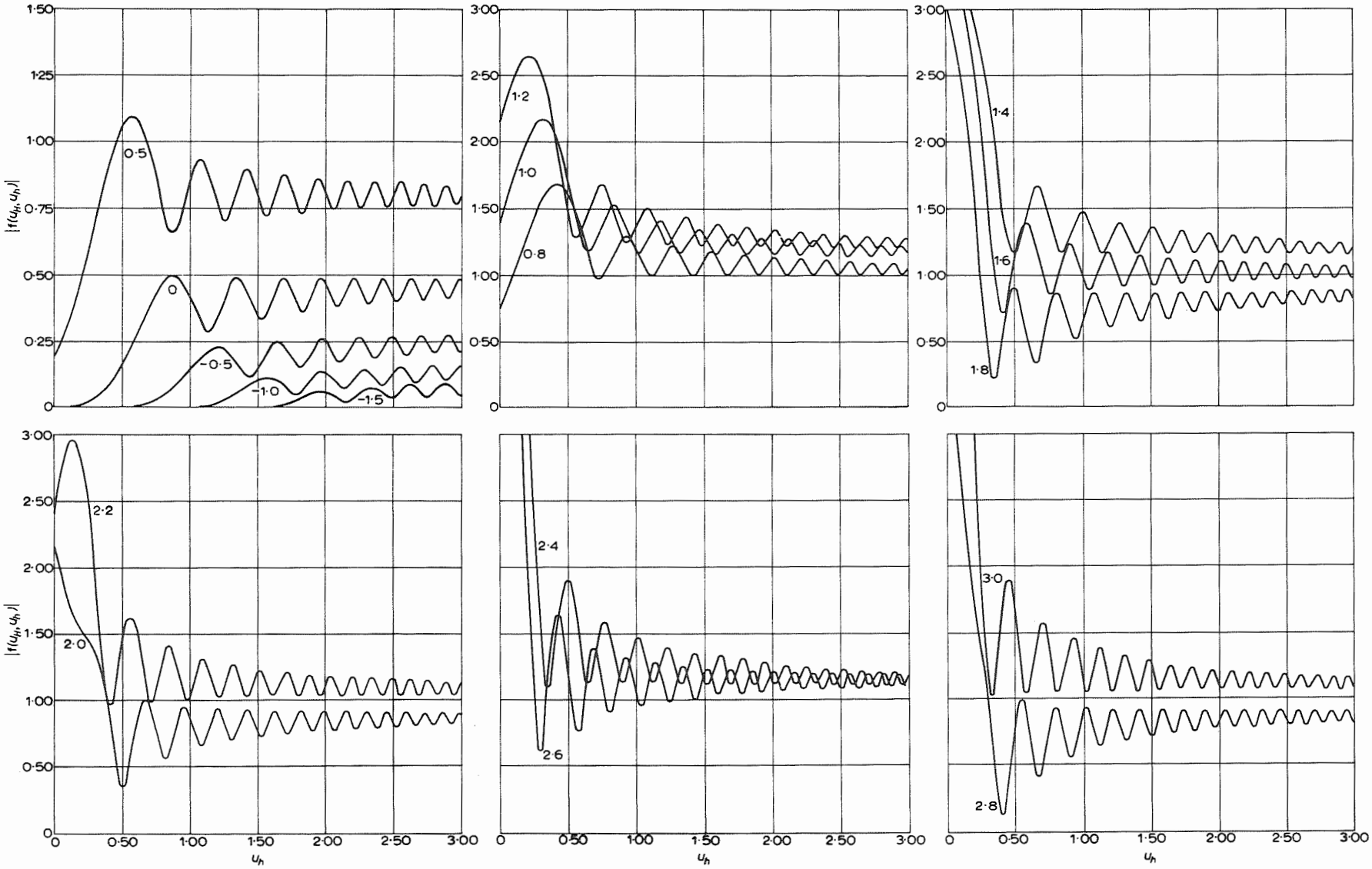

Fig. 12 - Modulus of $f(u_H, u_h)$

Numbers against curves denote values of $u_H - u_h$

For many applications the phase of $\rho(\phi)$ is of no interest and attention may be confined to the value of $|f(u_H,u_h)|$, which is equal to $|F|$ when $d_2 \gg d_1$ and related to it by Equation (27) when d_2 is comparable with d_1. In Fig. 12, computed values of $|f(u_H,u_h)|$ are plotted as a function of u_h for a number of different values of $u_H - u_h$.

The oscillatory nature of these curves is due to interference between direct and ground reflected illumination of the obstacle, one cycle corresponding to a one wavelength change in the path difference between direct and ground reflected rays from A_1 to the top of the obstacle. If the aerial and obstacle heights are increased but a constant height difference maintained the oscillations die out and the values of $|f(u_H,u_h)|$ tend to the values of $|F|$ given in Fig. 10.

The fact that $|f(u_H,u_h)|$ and therefore $|F|$ can be considerably greater than unity is a surprising result. Large values of $|F|$ occur when A_1 is close to the ground and the obstacle is somewhat higher. Under these conditions the direct signal arriving at the receiver is relatively weak (because of the low height of A_1) while the signal re-radiated from the upper part of the obstacle is enhanced because of its greater height. Large values of $|F|$ can only occur if the re-radiation from the upper part of the obstacle is substantially co-phased. If this requirement is not satisfied the net re-radiation from the upper part of the obstacle may be quite small and low values of $|F|$ obtained even with tall obstacles. As the height of an obstacle is increased the value of $|F|$ goes through a succession of maxima and minima and eventually tends to unity.

The curves of Fig. 12 cover a large part of the range of values of u_H and u_h which are encountered in practice, with the exception of values of u_h greater than 3. When u_h is large, however, the oscillations become relatively small and for most purposes the mean value about which each curve oscillates provides a sufficiently close approximation to the required value of $|f(u_H,u_h)|$. It may be shown that this mean value is given by

$$\frac{1}{\sqrt{2}} \left| \psi(u_H - u_h) + \tfrac{1}{2} - j\tfrac{1}{2} + \frac{j}{\pi u_h} e^{-j\pi(u_H - u_h)^2/2} \right| \qquad (29)$$

When u_h is very large, $|f(u_H,u_h)|$ is given approximately by the $u_A = 0$ curve in Fig. 10.

Values of F for obstacles illuminated by transmitting aerials having vertical directivity may be calculated by integrating the complex value of F, given by Equation (27) or (28) as appropriate, along the length of the aerial (as in Section 3.1) or by regarding the aerial as a set of discrete sources and calculating the average value of F. Fig. 13 shows an example of a computation of $|F|$ for an 8-source aerial, compared with values of $|F|$ for a single source at the same height as the centre of the directional aerial. The sources were spaced 1·0λ vertically and assumed to carry equal co-phased currents. The obstacle and aerial heights

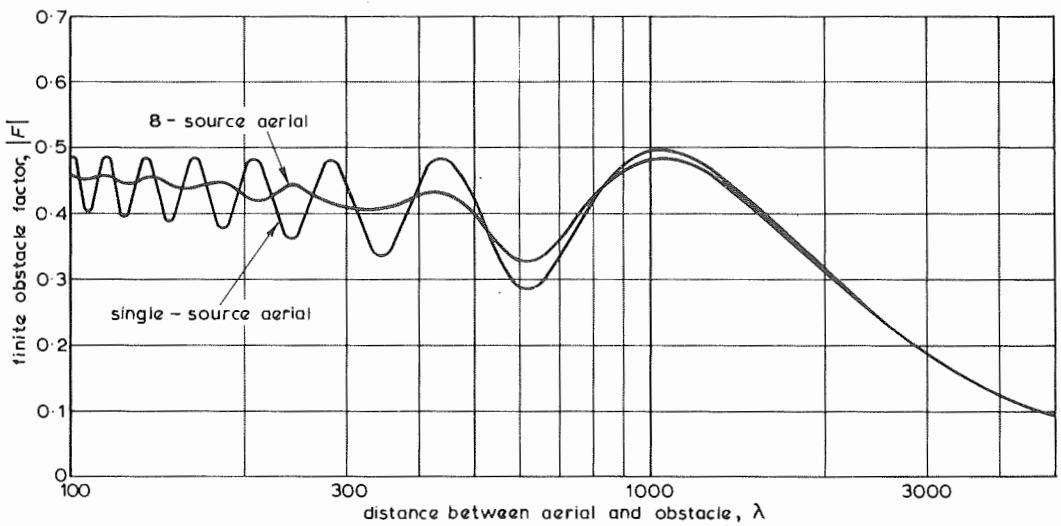

Fig. 13 - Comparison of finite obstacle factors for aerials with and without vertical directivity

Height of obstacle 20λ Height of centres of aerials 20λ Inter-tier spacing 1·0λ

were equal and the distance to the receiving aerial was assumed to be large compared with d_1.

The oscillations in both curves are due to interference between direct- and ground-reflected illumination of the obstacle, the maxima occurring when direct- and ground-reflected rays from the source are in phase near the top of the obstacle. With the directional aerial the oscillations are smaller than with a single source because of the reduction of the ground-reflected ray. If the directional aerial is considered in more detail we find that the first zero in its v.r.p. occurs at 7·2° and falls at the base of the obstacle when the distance is 160λ. For distances less than 160λ the ground-reflected illumination of the obstacle is therefore insignificant and the oscillations are small. The value of $|F|$ is then a little less than 0·5 (the value which would be expected for an aerial and obstacle of equal height) because linear height-gain diminishes the contribution to the distant field strength from the lower part of the obstacle. Fig. 13 shows that ground-reflected illumination is still unimportant at distances somewhat greater than 160λ; this is because the upper part of the obstacle is not strongly illuminated by the ground-reflected ray. At distances greater than 320λ, however, the whole of the obstacle and its image lies within the main lobe of the directional aerial and consequently there is less difference between the two curves.

The single source curve of Fig. 13 is similar to the $u_H - u_h = 0$ curve of Fig. 12, the only difference being that $|F|$ is plotted as a function of d/λ instead of u_h. For $d < 320\lambda$ the value of $|F|$ for the directional aerial is closely approximated to by the values for $u_H - u_h = 0$ given by Equation (29). This result suggests that Equation (29) may be used for other aerial and obstacle heights when directional aerials are used, provided the obstacle is not strongly illuminated by ground-reflected radiation.

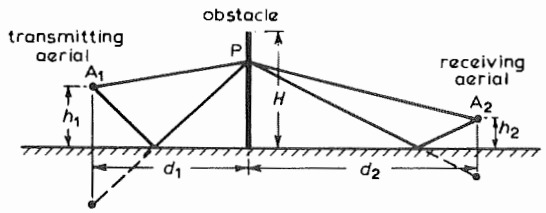

Fig. 14 - Obstacle and aerials, showing direct and ground-reflected rays

3.2.2. Distance to Receiving Aerial Insufficient for Linear Height-Gain

The arrangement considered is shown in Fig. 14, the obstacle and the two aerials not necessarily being in the same vertical plane. As in the previous sections, the ground is assumed to be flat and to have a reflexion coefficient of -1; this assumption is reasonable at all angles of incidence for horizontal polarization, and for angles of incidence greater than 70° for vertical polarization. Aerial A_1 is assumed to be transmitting.

The total re-radiated field strength at A_2 due to the current induced in the obstacle by A_1 is found by integrating along the length of the obstacle. The current at P (Fig. 14) is induced by the resultant of direct- and ground-reflected radiation from A_1, while the re-radiated field strength at A_2 is itself the resultant of direct- and ground-reflected radiation from P. Consequently the field at A_2 may be regarded as the resultant of four components, corresponding to the four paths shown in Fig. 15.

The component E_a due to direct illumination of the obstacle and direct re-radiation is given by an expression similar to Equation (3) and is

$$E_a = -jKg(\phi) \int_{-L}^{H-L} \frac{e^{-j\beta(r_1 + r_2)}}{r_1 r_2}\, dz \qquad (30)$$

where r_1 and r_2 are the distances shown in Fig. 15(*a*) and L is the height at which the line A_1A_2 intersects the obstacle.

Making the usual approximations, Equation (30) may be re-written

$$E_a = -j \frac{K\, g(\phi)}{d_1 d_2}\, e^{-j\beta(d_1 + d_2 + \delta)} \int_{-L}^{H-L} e^{-j\beta z^2/2d}\, dz \qquad (31)$$

where δ is the difference between the oblique distance A_1A_2 and the horizontal distance $(d_1 + d_2)$.

The corresponding expressions for the other three components are

$$E_b = j \frac{K\, g(\phi)}{d_1 d_2}\, e^{-j\beta(d_1 + d_2 + \delta')} \int_{-L'}^{H-L'} e^{-j\beta z^2/2d}\, dz \qquad (32)$$

$$E_c = j \frac{K\, g(\phi)}{d_1 d_2}\, e^{-j\beta(d_1 + d_2 + \delta')} \int_{L'}^{H+L'} e^{-j\beta z^2/2d}\, dz \qquad (33)$$

$$E_d = -j \frac{K\, g(\phi)}{d_1 d_2} e^{-j\beta(d_1 + d_2 + \delta)} \int_{L}^{H+L} e^{-j\beta z^2/2d} dz \qquad (34)$$

where L' is the height of intersection of the line A_1A_2' and the obstacle (Fig. 15(*b*)) and δ' is the difference between A_1A_2' and $d_1 + d_2$.

It may be shown that the sum of the four components is

$$E_R = -j \frac{Kg(\phi)}{d_1 d_2} (\lambda d)^{1/2}\, Q\, e^{-j\beta(d_1 + d_2)} \qquad (35)$$

where

$$Q = \frac{1}{\sqrt{2}} \{ e^{-j\beta\delta} [\psi(u_H - u_L) + \psi(u_H + u_L)] - e^{-j\beta\delta'} [\psi(u_H - u_L') + \psi(u_H + u_L')] \} \qquad (36)$$

$$u_H = \frac{H/\lambda}{(d/2\lambda)^{1/2}} \qquad u_L = \frac{L/\lambda}{(d/2\lambda)^{1/2}} \qquad u_L' = \frac{L'/\lambda}{(d/2\lambda)^{1/2}}$$

and $\psi(u)$ is the complex Fresnel integral.

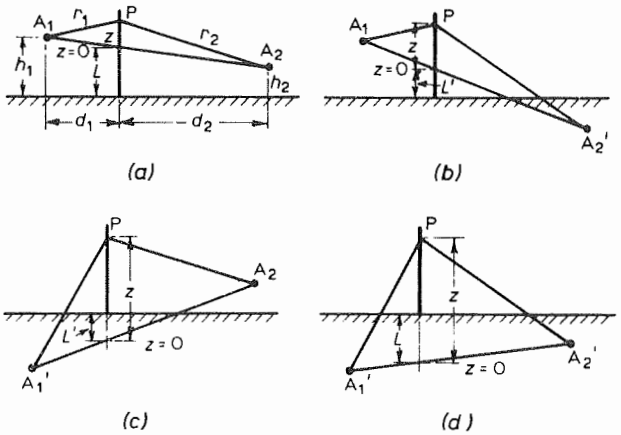

Fig. 15 - The four rays which contribute to re-radiation from an obstacle

The field strength due to direct radiation is the sum of direct- and ground-reflected waves, each of which is given by Equation (1). Their resultant is

$$E_D = j \frac{2K}{d_0} \sin\left(\frac{\beta h_1 h_2}{d_0}\right) e^{-j\beta(d_0 + \delta_0)} \qquad (37)$$

where $\delta_0 = (h_1^2 + h_2^2)/2d_0$

From Equations (35) and (37), the re-radiation coefficient is

$$\rho(\phi) = \frac{E_R}{E_D} = -\frac{g(\phi)\, d_0}{2d_1 d_2} (\lambda d)^{1/2}\, Q\, \mathrm{cosec}\left(\frac{\beta h_1 h_2}{d_0}\right) e^{-j\beta(d_1 + d_2 - d_0 - \delta_0)} \qquad (38)$$

From Equations (5) and (38) the finite obstacle factor is

$$F = \frac{\rho(\phi)}{\rho_0(\phi)} = \frac{j}{2} Q\, \mathrm{cosec}\left(\frac{\beta h_1 h_2}{d_0}\right) e^{j\pi/4}\, e^{j\beta\delta_0} \qquad (39)$$

Equations (38) and (39) contain so many parameters that presentation in graphical form is impracticable. To enable specific values of $|\rho(\phi)|$ to be calculated, however, a computer programme has been developed for the function

$$\left| \frac{d_0}{2d_1 d_2} (\lambda d)^{1/2}\, Q\, \mathrm{cosec}\left(\frac{\beta h_1 h_2}{d_0}\right) \right|$$

This function is referred to as the "obstacle re-radiation factor". The input data required are h_1, h_2, H, d_0, d_1 and d_2, all in wavelengths.

3.3. Obstacle at Great Distance from Both Aerials

In this section we consider an obstacle which is so far from the transmitting aerial that the illuminating field strength increases linearly with height and is so far from the receiving aerial that the linear height-gain condition is also satisfied for re-radiation. In this situation reflected signals causing multipath distortion may be important but shadow losses are insignificant and the absolute phase of the re-radiated signal is therefore of no interest.

The field strength $E(z)$ which would exist at the obstacle if it were not there is the sum of direct- and ground-reflected waves each given by Equation (1). Their resultant is given approximately by

$$E(z) = j\, 2K \frac{\beta h_1 z}{r_1^2} e^{-j\beta r_1} \qquad (40)$$

where z is measured from ground level and r_1 from the point on the ground below A_1.

The re-radiated field strength from an element of the obstacle is the sum of direct- and ground-reflected waves each given by Equation (2) and is approximately equal to

$$E_R = 2\, g(\phi) \frac{\beta h_2 z}{r_2^2} e^{-j\beta r_2} E(z)\, \delta z \qquad (41)$$

where r_2 is measured from the ground below A_2, as in Fig. 11.

Combining Equations (40) and (41), making the usual approximations and integrating, we have

$$E_R = j4K\,g(\phi)\,\frac{\beta^2 h_1 h_2}{d_1^2 d_2^2}\,e^{-j\beta(d_1+d_2)}\int_0^H z^2 e^{-j\beta z^2/2d}\,dz \qquad (42)$$

This leads to the result

$$|E_R| = \left|4K\,g(\phi)\,\frac{h_1 h_2}{d_1^2 d_2^2}\,\beta d\left(\frac{\lambda d}{2}\right)^{1/2} \times\left[\psi(u_H) - u_H e^{-j\pi u_H^2/2}\right]\right| \qquad (43)$$

The field strength due to direct radiation is given by an expression similar to Equation (40); the ratio of $|E_R|$ and $|E_D|$ gives $|\rho(\phi)|$ as follows,

$$|\rho(\phi)| = \left|2\,g(\phi)\left(\frac{d_0}{d_1 d_2}\right)^2 d\left(\frac{\lambda d}{2}\right)^{1/2} \times\left[\psi(u_H) - u_H e^{-j\pi u_H^2/2}\right]\right|$$

It will be seen that $|\rho(\phi)|$ is independent of h_1 and h_2.

If $r_1 + r_2$ does not exceed $d_1 + d_2$ by more than $\lambda/4$ at the top of the obstacle, the exponential term within the integral of Equation (42) may be disregarded. The expression for $|\rho(\phi)|$ then simplifies to

$$|\rho(\phi)| = |g(\phi)|\,\frac{4\pi H^3}{3\lambda}\left(\frac{d_0}{d_1 d_2}\right)^2$$

provided H is less than $(\lambda d/2)^{1/2}$.

4. RE-RADIATION FROM NON-UNIFORM OBSTACLES

Although the re-radiation coefficient of a non-uniform obstacle such as a tapered self-supporting tower would be difficult to calculate exactly, since $g(\phi)$ is not constant, an approximate solution may be obtained by ascribing an average value to $g(\phi)$. Now the part of the obstacle which makes the major contribution to the re-radiated field is the stationary phase region, i.e. the part of the obstacle responsible for the component of the re-radiated field which has the least delay. This is the part of the obstacle which is intersected by the lines joining A_1 and A_2 or their images. Thus in the general case illustrated in Fig. 15 the calculation should be based on the average value of $g(\phi)$ between heights L and L'.

Stayed masts may also be regarded as non-uniform obstacles, the effects of individual stay wires being considered separately. Since the width of a stay wire is always small compared with the wavelength its re-radiation pattern must be symmetrical about its axis. It therefore takes the form of a cone, as shown in Fig. 16. In the horizontal direction significant re-radiation occurs only in the shadow direction and in the direction corresponding to specular reflexion from the plane containing the mast and the stay wire. In other directions the re-radiation is directed above or below the horizontal and has little effect except in the immediate vicinity of the mast.

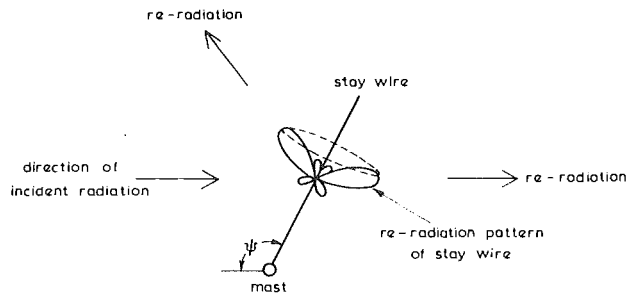

Fig. 16 - Plan view showing re-radiation from a stay wire

To estimate the effect of a stay wire, the incident electric vector is resolved into components parallel and perpendicular to the wire. The re-radiated field is then calculated with the help of Fig. 3(*a*), the parallel component being regarded, for this purpose, as a vertically-polarized incident wave.* The amplitude of the component of the re-radiated field which has the same polarization as the incident wave is then determined. This double process of resolving into component vectors has the effect of multiplying the value of $g(\phi)$ obtained from Fig. 3(*a*) by $\cos^2\theta$ for vertical polarization and by $\sin^2\theta\,\sin^2\psi$ for horizontal polarization, where θ is the angle of inclination of the stay wire to the vertical and ψ is the angle shown in Fig. 16. The multiplying factors show that the re-radiation from a stay wire is independent of its position around the mast for vertical polarization.

Since the width of a stay is small compared with that of the mast it supports, its effect will generally be much smaller than that of the mast it supports. However, when there are several stay wires in the same vertical plane their re-radiation will add in phase in the directions shown in Fig. 16. They may therefore produce an appreciable effect. Furthermore, in the shadow direction ($\phi = \pi$), the effects of all the stays will add in phase and combine with the mast in opposing the incident radiation.

* For $\beta a < 0{\cdot}1$, $|g(\phi)|$ is approximately equal to $1/[2\log(1{\cdot}123/\beta a)]$.

5. THE EFFECT OF THE INTERVENING TERRAIN

In Section 3 the ground was assumed to be perfectly level and to have a reflexion coefficient of -1 at all angles of incidence. The effect of departures from this idealized situation are now discussed.

Although -1 is a good approximation to the ground reflexion coefficient for horizontally-polarized waves at all frequencies and angles of incidence, it applies only near grazing incidence with vertical polarization. Consequently the illumination of an obstacle by an aerial at a moderate distance (as in Section 3.2) may be somewhat different for the two polarizations. On the other hand reception at a distant receiving aerial (as in Section 3.2.1) will not be influenced greatly by the polarization.

The effect of a departure of the ground reflexion coefficient from -1 may be assessed qualitatively by considering Fig. 13. As already stated, the oscillations in the curve for the single source are due to interference between direct- and ground-reflected illumination of the top of the obstacle and, as Fig. 13 shows, the oscillations are reduced when the reflected wave is diminished by increased aerial directivity. A similar effect will occur if the ground reflexion coefficient is reduced, but if its phase is changed and its amplitude not greatly diminished, the oscillations will be displaced sideways. In the absence of a detailed calculation it is reasonable to assume that $|F|$ or $|\rho(\phi)|$ is equal to the mean value of the appropriate oscillating curve, with a tolerance equal to the amplitude of the oscillations.

Surface roughness has an effect similar to that of reducing the ground reflexion coefficient. The effect is greatest at high frequencies and least at angles of incidence close to the horizontal. As a rough guide, Rayleigh's criterion may be used; this states that a surface may be regarded as smooth if the heights of the ground irregularities in wavelengths are less than $0{\cdot}125/\cos\theta$, where θ is the angle of incidence.

Larger irregularities such as hills may considerably modify the re-radiation coefficient of an obstacle. For example, it is possible to visualise a situation in which an obstacle is strongly illuminated by the transmitting aerial and is also visible from the receiving aerial although the two aerials are screened from each other by an intervening hill; the re-radiation coefficient would then be considerably enhanced. This kind of situation is most likely to arise when d_1 and d_2 are comparable. When $d_1 \ll d_2$, the propagation paths from both A_1 and the obstacle to the distant aerial will be similar and the direct and re-radiated waves will be attenuated to an equal extent.

It is difficult to calculate the re-radiation coefficient in a situation of the type described above. A crude estimate may be made, however, by calculating $\rho(\phi)$ assuming the ground to be flat and then increasing this value to allow for the extra attenuation caused by the hill between the two aerials.

A different situation arises when the obstacle is on higher ground than the transmitting aerial. The re-radiation is then enhanced by the greater height-gain of the obstacle and diminished by the fact that the re-radiation tends to be predominantly above the horizontal plane. An exact analysis of this situation would follow the lines described in Section 3.2, the integrations being performed between different limits. A crude estimate may be made by comparing the lengths of rays drawn from one aerial to the other via the top and bottom of the obstacle with the length A_1A_2 (Fig. 15); this enables the number of Fresnel zones which lie on the obstacle to be estimated and its effect assessed. If the obstacle is situated on lower ground its effect is likely to be small unless it intersects the line A_1A_2.

6. CALCULATION OF THE DISTURBANCES CAUSED BY AN OBSTACLE

Having determined the re-radiation coefficient of an obstacle in a number of horizontal directions, its effect on the service provided by the transmitting aerial may be assessed.

The disturbing effects caused by an obstacle may be classified under three headings:

(1) Distortion of the shape of the horizontal radiation pattern (h.r.p.) of the transmitting aerial i.e. unwanted variations of effected radiated power (e.r.p.) with direction, which may give inadequate reception in some directions and the possibility of interference to co-channelled transmissions in other directions.

(2) Variation of field strength over the working frequency band in a fixed direction.

(3) Distortion in television pictures or in f.m. sound reproduction caused by reflected signals of appreciable delay.

These three forms of distortion are discussed in greater detail below.

6.1. Distortion of the H.R.P.

As an example, Fig. 17 shows the h.r.p. of a typical aerial in the presence of an obstacle for which $|\rho(\phi)| = 0{\cdot}12$ at $\phi = 180°$ and 0·06 between $\phi = 0$ and $\phi = 90°$. The distance between aerial and obstacle is 30 wavelengths and the distance to the receiving aerial assumed to be very much greater.

In the shadow region ($\phi = 180°$) the obstacle reduces the field strength radiated by the aerial from 1·00 to 0·88, a reduction of 1·1 dB. A movement by the observer of 10° either way from $\phi = 180°$ changes the relative phase of the direct and re-radiated signals by 180°, so that they add in phase to give a relative field strength of 1·12 (an increase of 1·0 dB). The amplitude of the re-radiated wave falls gradually to 0·06 at $\phi = 90°$ and then remains at this value. The field-strength variations become more rapid as $\phi = 90°$ is approached but become slower again as the observer continues towards $\phi = 0$. They are so rapid that it is impossible to show them on Fig. 17 in the $\phi = \pm 90°$ directions. Nor are they shown in the $\phi = 0$ direction because here the phase difference between the direct and re-radiated waves depends on the exact spacing between aerial and obstacle and on the phase variation of their radiation patterns; these factors are not normally known with sufficient accuracy. In these directions, therefore, the variations of the h.r.p. can only be indicated by upper and lower limits.

It should be noted that, although the amplitude of the re-radiation from the mast remains constant at 0·06 over an arc of 180° centred on $\phi = 0$, its amplitude relative to the direct radiation varies because the aerial does not radiate uniformly in all directions. Thus the field-strength variations at $\phi = 0$ are ±0·5 dB (1·00 ±0·06), at $\phi = 90°$ they are ±0·7 dB (0·82 ±0·06) and at $\phi = -90°$ they range between +2·0 dB and -2·5 dB (0·24 ± 0·06).

Strictly speaking, field-strength variations occur only if the transmitter is unmodulated or if the time variation of its modulation is slow compared with the time delay of the re-radiated wave. If this is not the case, the re-radiation takes the form of a delayed signal; this is discussed in Section 6.3.

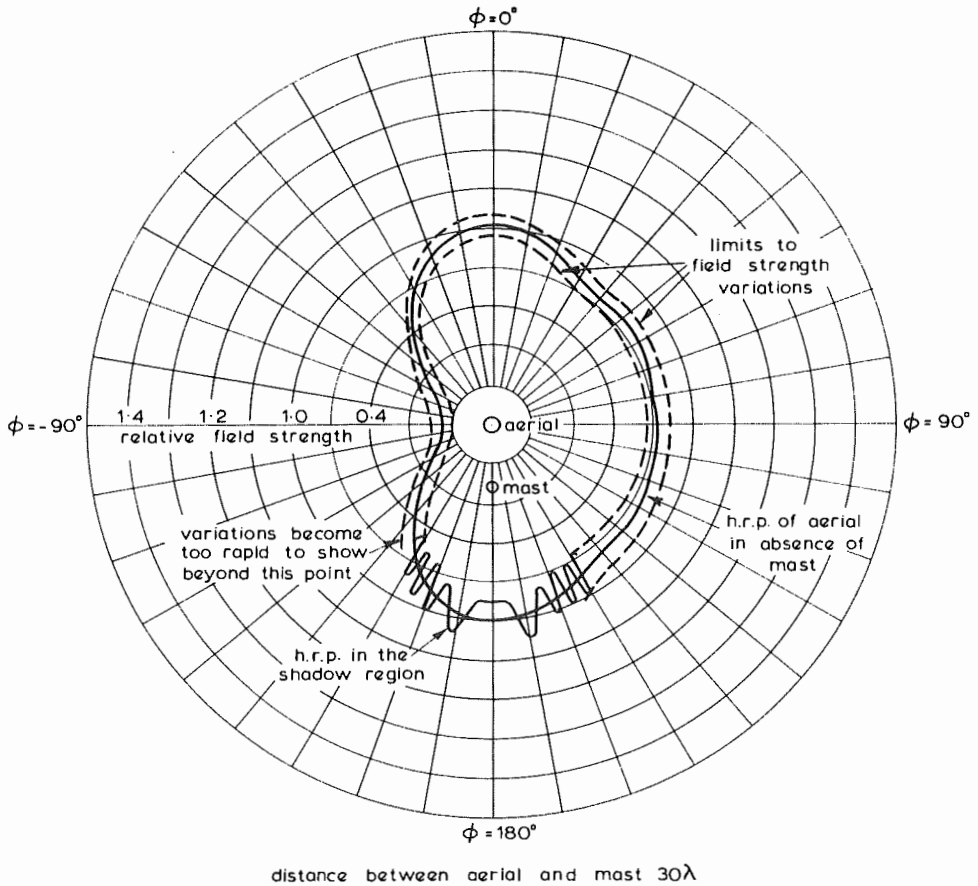

Fig. 17 - The h.r.p. of an aerial in the presence of an obstacle mast

6.2. Variation of Field Strength over the Working Frequency Band

In the case illustrated in Fig. 17 (where the spacing between aerial and obstacle is 30λ) the path difference between the direct and re-radiated waves increases from zero at $\phi = 180°$ to 60λ at $\phi = 0$. Thus, at $\phi = 0$, a 1% change in frequency will change the path difference between the direct and re-radiated waves by about $0{\cdot}5\lambda$ and change their relative phase by 180°. As 1% is only a fraction of the bandwidth occupied by a television transmission on Bands I and III, the video signal received at a fixed point will vary over the band by exactly the same amount that the field strength varies if the observer moves. Thus at $\phi = -90°$, the video response would vary by 4·5 dB over the band; this could cause appreciable distortion. Similarly the re-radiated wave can disturb the sound/vision ratio of a television transmission, and may upset the parity between the different programmes radiated by a v.h.f. sound broadcasting station.

6.3. Distortion caused by Re-radiated Waves having Appreciable Delay

If the time delay between the direct and re-radiated waves exceeds the time occupied by a picture element of a television transmission, the re-radiation may be visible as an edge effect or as a separate image or "ghost". This may be either positive or negative, depending on the relative phase of the two waves.

In the example illustrated in Fig. 17, if the spacing between the aerial and obstacle is 500 ft (150 m), the time delay can have a maximum value of 1 μs at $\phi = 0$ and half this value at $\phi = \pm 90°$. This is sufficient for the distortion to be visible as a delayed image on a 405-line picture. The relative amplitude of the delayed image is equal to the ratio of the direct and re-radiated waves. Thus it is 0·06/1·00 (-24 dB) at $\phi = 0$, 0·06/0·82 (-23 dB) at $\phi = 90°$ and 0·06/0·24 (-12 dB) at $\phi = -90°$. These levels would normally be regarded as unacceptable.

In the case of f.m. sound broadcasting, delayed re-radiation can cause multipath distortion.[12]

7. CONCLUSIONS

The theory presented in this report shows that the strength of a signal re-radiated by an obstacle situated near an aerial decreases inversely as the square root of the aerial-to-obstacle distance, provided ground reflexions may be neglected and the obstacle is much higher than the aerial. If the height of the aerial is equal to that of the obstacle, the amplitude of the re-radiated signal is halved; it decreases rapidly if the aerial height is increased still further. Ground reflexions also modify the re-radiated signal and under some circumstances may make it appreciably stronger than it would be in the absence of reflexions.

The strength of the re-radiated signal also depends on the size and shape of the obstacle. If the obstacle is a uniform solid cylinder whose width exceeds one wavelength, its re-radiating properties may be determined by the methods of geometrical optics. Thus the re-radiation in the shadow direction is concentrated in a lobe which resembles that due to a radiating aperture of the same width as the obstacle. The width of this lobe (for a given obstacle size) decreases as the frequency increases, while the strength of the re-radiated signal increases as the square root of the frequency if certain conditions are satisfied. Lobes with similar properties are also formed when specular reflexion takes place from the faces of polygonal cylinders. Reflexion from a circular cylinder, however, is almost constant over a wide arc and is independent of frequency.

The behaviour of lattice structures is more complicated and must generally be determined experimentally. Brick and concrete structures of sufficient size behave as metallic obstacles where shadowing is concerned, but in other directions the re-radiation is approximately halved. Reinforced concrete structures resemble metallic obstacles.

The theory applies to re-radiation from uniform obstacles situated on level ground whose reflexion coefficient is assumed to be -1 over a wide range of angles. As this idealized state of affairs is seldom encountered in practice, it is proposed to carry out measurements near real obstacles to see how well the theory is obeyed in typical situations. Consideration is also being given to the possibility of performing other measurements with models in order to test the theory more exactly.

8. REFERENCES

1. MEGAW, E.C.S. 1947. Some effects of obstacles on the propagation of very short radio waves. *J. Instn elect. Engrs*, 1948, **95**, III, 34, pp. 97 - 105.

2. CARTER, P.S. 1941. Antenna arrays around cylinders. *Proc. Inst. Radio Engrs*, 1943, **31**, 12 p. 671 - 693.

3. MEI, K.K. *and* VAN BLADEL, J.G. 1962. Low-frequency scattering by rectangular cylinders. *I.E.E.E. Trans Antennas & Propagn*, 1963, **AP-11**, 1, pp. 52 - 56.

4. MEI, K.K. *and* VAN BLADEL, J.G. 1962. Scattering by perfectly-conducting rectangular cylinders. *I.E.E.E. Trans Antennas & Propagn*, 1963, **AP-11**, 2, pp. 185 - 192.

5. HILL, P.C.J. 1964. The measurement of re-radiation from lattice masts at v.h.f. *Proc. Instn elect. Engrs*, 1964, **111**, 12, pp. 1957 - 1968.

6. HIMBURG, L.F. 1959. Uber den Beugungseinfluss eines Zylinders im Strahlungsfeld eines UKW-Senders. *Institut für Rundfunktechnik, Hamburg*. Bericht No. 26, October 1959.

7. Reflexions from masts at very high frequencies. Research Department Technical Memorandum No. E-1065, December 1961.

8. BLYTHE, J.H. 1962. Shadowing produced by a cylindrical tower near to a transmitting tower. *I.E.E.E. Trans Antennas & Propagn*, 1963, **AP-11**, 3, pp. 376 - 377.

9. OTAKE, T. 1912. Calculation of electrostatic capacities of long straight cylinders with some geometrical cross-section. *Kyushu University College of Engineering Memoirs*. 1913, **1**, 1, pp. 31 - 77.

10. SMYTHE, W.R. 1939. Static and dynamic electricity. New York, McGraw-Hill, 1939, Chapter 4.

11. The power loss from open-wire high-frequency transmission lines due to support structures. Research Department Report No. E-079, Serial No. 1962/52.

12. HARVEY, R.V. 1960. V.H.F. sound broadcasting. *Proc. Instn elec. Engrs*, 1960, **107B**, 35, pp. 412 - 422.

9. APPENDICES

9.1. The Re-radiation Coefficient of a Perfectly-Conducting Circular Cylinder

The re-radiation coefficient of an infinite circular cylinder may be conveniently derived from Carter's formulae[2] for the far field radiation pattern of a source A_1 in the presence of the cylinder shown in Fig. 18. For vertical polarization the source is a vertical doublet and the horizontal radiation pattern is given by

$$E = V_0 + 2 \sum_{n=1}^{\infty} j^n V_n \cos n\phi \qquad (44)$$

where

$$V_n = J_n(\beta d_1) - J_n(\beta a) \frac{H_n^{(2)}(\beta d_1)}{H_n^{(2)}(\beta a)}$$

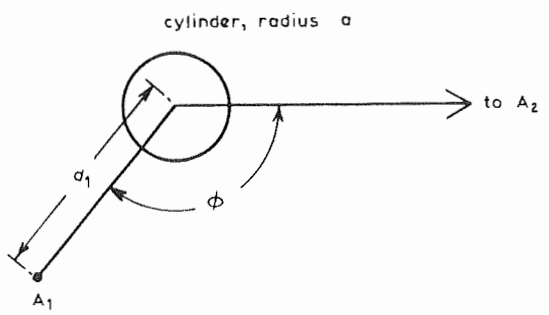

Fig. 18 - Re-radiation from a circular cylinder

The phase of radiation pattern is referred to the cylinder axis.

Now if the cylinder were removed, the field which the doublet would radiate would be constant in amplitude in all directions, but if its phase were still referred to the position occupied by the cylinder axis, it would be given by the expression

$$E_D = e^{-j\beta d_1 \cos\phi}$$

$$= J_0(\beta d_1) + 2 \sum_{n=1}^{\infty} j^n J_n(\beta d_1) \cos n\phi \qquad (45)$$

The contribution to the total field due to the re-radiation from the cylinder alone is equal to the difference between Equations (44) and (45) and is therefore given by

$$E_R = -J_0(\beta a) \frac{H_0^{(2)}(\beta d_1)}{H_0^{(2)}(\beta a)}$$

$$- 2 \sum_{n=1}^{\infty} j^n J_n(\beta a) \frac{H_n^{(2)}(\beta d_1)}{H_n^{(2)}(\beta a)} \cos n\phi \qquad (46)$$

By definition the re-radiation coefficient is equal to the ratio of the direct and re-radiated fields; from Equations (45) and (46) this is given by

$$\rho_0(\phi) = \frac{E_R}{E_D} = -e^{-j\beta d_1 \cos\phi} \left[J_0(\beta a) \frac{H_0^{(2)}(\beta d_1)}{H_0^{(2)}(\beta a)} + 2 \sum_{n=1}^{\infty} j^n J_n(\beta a) \frac{H_n^{(2)}(\beta d_1)}{H_n^{(2)}(\beta a)} \cos n\phi \right] \quad (47)$$

Using a similar method it may be shown that the re-radiation coefficient for horizontally-polarized waves is given by

$$\rho_0(\phi) = e^{-j\beta d_1 \cos\phi} \left[J_0'(\beta a) \frac{H_0^{(2)}(\beta d_1)}{H_0^{(2)'}(\beta a)} + 2 \sum_{n=1}^{\infty} j^n J_n'(\beta a) \frac{H_n^{(2)}(\beta d_1)}{H_n^{(2)'}(\beta a)} \cos n\phi \right] \quad (48)$$

Equation (48) applies to an omnidirectional source (i.e. a horizontal loop aerial). If the source were a horizontal dipole facing the cylinder, the expression for $\rho(\phi)$ would be similar, but the Hankel functions of βd_1 would be replaced by their derivatives. Both expressions lead to Equation (13) when $d_1/\lambda \gg (a/\lambda)^2$.

9.2. Reflexion from a Large Circular Cylinder

In directions other than the shadow region ($\phi = \pi$) waves falling on a circular cylinder are reflected and suffer attenuation because of angular divergence. When the cylinder radius is sufficiently large, geometrical optics may be used to calculate this attenuation and derive a value for $\rho_0(\phi)$.

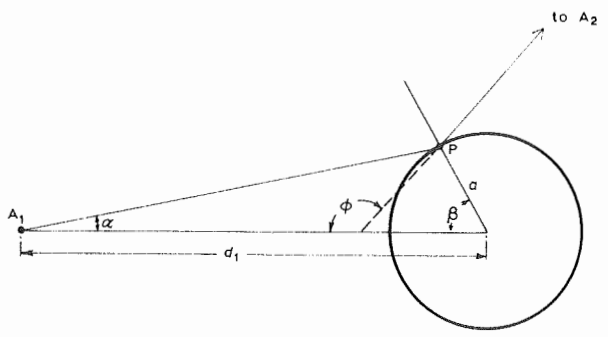

Fig. 19 - Reflexion from a large circular cylinder

Fig. 19 shows a source A_1 distant d_1 from a cylinder of radius a. P is the reflexion point corresponding to the angle ϕ; it subtends angles α at A_1 and β at the cylinder axis. The distance to aerial A_2 is very much greater than d_1.

A bundle of incident rays of angular width $\delta\alpha$ spreads over a wider angle $\delta\phi$ after reflexion and the intensity of the reflected ray is reduced by the factor $d\alpha/d\phi$. The ratio of the field strengths of the direct and reflected waves arriving at A_2 is the square root of this quantity.

From geometrical considerations it may be shown that $\beta = \frac{1}{2}(\phi - \alpha)$ and also that $\sin\beta \simeq \alpha d_1/a$, provided $d_1 \gg a$. It therefore follows that

$$\frac{\alpha d_1}{a} \simeq \sin\frac{\phi - \alpha}{2} \simeq \sin\frac{\phi}{2} - \frac{\alpha}{2}\cos\frac{\phi}{2} \quad (49)$$

Differentiating Equation (49) with respect to ϕ we have

$$\left(\frac{d_1}{a} + \frac{1}{2}\cos\frac{\phi}{2}\right)\frac{d\alpha}{d\phi} \simeq \frac{1}{2}\cos\frac{\phi}{2} + \frac{\alpha}{4}\sin\frac{\phi}{2} \quad (50)$$

Since $d_1/a \gg \frac{1}{2}\cos(\phi/2) \gg (\alpha/4)\sin(\phi/2)$ for all values of ϕ except those corresponding to the shadow region ($\phi \simeq \pi$), Equation (50) may be simplified:

$$\frac{d\alpha}{d\phi} \simeq \frac{a}{2d_1}\cos\frac{\phi}{2} \quad (51)$$

The modulus of the re-radiation coefficient is therefore

$$|\rho_0(\phi)| = \left(\frac{d\alpha}{d\phi}\right)^{\frac{1}{2}} \simeq \left(\frac{a}{2d_1}\cos\frac{\phi}{2}\right)^{\frac{1}{2}} \quad (52)$$

and it follows that

$$|g(\phi)| = |\rho_0(\phi)| \left(\frac{d_1}{\lambda}\right)^{\frac{1}{2}} = \frac{1}{2}\left(\frac{2a}{\lambda}\cos\frac{\phi}{2}\right)^{\frac{1}{2}} \quad (53)$$

9.3. Re-radiation from Rectangular Cylinders of Intermediate Size

In Reference 4, curves for two quantities termed "gain" and "scattering cross section" are presented. The gain G_E is defined as

$$G_E = \frac{\text{scattered power density in a given direction}}{\text{average scattered power density}} \quad (54)$$

The published curves showing gain as a function of azimuth are therefore power radiation patterns. The scattering cross section* σ_{sc} is defined as

$$\sigma_{sc} = \frac{\text{scattered power per unit length of cylinder}}{\text{incident power density}} \tag{55}$$

The relation between these two quantities and $g(\phi)$ may be derived as follows:

The average scattered power density at a distance r from the axis of the cylinder is equal to the scattered power per unit length divided by $2\pi r$. From Equation (55) we therefore have

$$\frac{\sigma_{sc}}{2\pi r} = \frac{\text{average scattered power density at distance } r}{\text{incident power density}} \tag{56}$$

From Equations (54) and (56) it will be seen that the scattered power density at a distance r in a particular direction, relative to the incident power density, is therefore $G_E\ \sigma_{sc}/2\pi r$; the modulus of the re-radiation coefficient is the square root of this quantity. We then have

$$\begin{aligned} |g(\phi)| &= \left(\frac{G_E\ \sigma_{sc}}{2\pi r}\right)^{1/2} \left(\frac{r}{\lambda}\right)^{1/2} \\ &= \frac{1}{\pi}\left[G_E\left(\frac{\sigma_{sc}}{4a}\right)\beta a\right]^{1/2} \end{aligned} \tag{57}$$

where $2a$ is the width of one face of the rectangular-section cylinder. Reference 4 contains curves giving G_E as a function of ϕ and $(\sigma_{sc}/4a)$ as a function of βa for rectangular cylinders with various aspect ratios; $g(\phi)$ may be calculated by substituting values from these curves in Equation (57).

* The scattering cross section of Reference 4 should not be confused with the scattering cross section of a finite object (sometimes called the "radar cross section"), which is defined as the ratio $4\pi r^2 W_r/W_i$, where W_r is the scattered power density at a distance r and W_i is the incident power density.

Printed by BBC Research Department, Kingswood Warren, Tadworth, Surrey